GEOPHYSICS, VOL. 54, NO. 6 (JUNE 1989); P. 680-688, 12 FIGS.

Amplitude-versus-offset variations in gas sands

Steven R. Rutherford* and Robert H. Williams‡

ABSTRACT

Seismic reflections from gas sands exhibit a wide range of amplitude-versus-offset (AVO) characteristics. The two factors that most strongly determine the AVO behavior of a gas-sand reflection are the normal incidence reflection coefficient R_0 and the contrast in Poisson's ratio at the reflector. Of these two factors, R_0 is the least constrained. Based on their AVO characteristics, gas-sand reflectors can be grouped into three classes defined in terms of R_0 at the top of the gas sand.

Class 1 gas sands have higher impedance than the encasing shale with relatively large positive values for R_0. Class 2 gas sands have nearly the same impedance as the encasing shale and are characterized by values of R_0 near zero. Class 3 sands have lower impedance than the encasing shale with negative, large magnitude values for R_0. Each of these sand classes has a distinct AVO characteristic.

An example of a gas sand from each of the three classes is presented in the paper. The Class 1 example involves a Hartshorn channel sand from the Arkoma Basin. The Class 2 example considers a Miocene gas sand from the Brazos offshore area of the Gulf of Mexico. The Class 3 example is a Pliocene gas sand from the High Island offshore area of the Gulf of Mexico.

INTRODUCTION

Amplitude-versus-offset (AVO) analysis (Ostrander, 1982, 1984) was initially proposed as a technique for validating seismic amplitude anomalies associated with gas sands. Most of the time, the gas sands that produce these amplitude anomalies have lower impedance than the encasing shales and have reflections that increase in magnitude with offset. These types of gas sands account for a large percentage of the AVO analyses being done in the industry.

Since the early days of AVO analysis, explorationists have learned that a wide range of AVO characteristics is possible for gas-sand reflections and that AVO analysis can be useful for analyzing reflections that do not necessarily correspond to "bright spots" on stacked seismic data.

This paper presents three examples that span the range of AVO effects associated with gas sands normally encountered in exploration. The examples belong to three classes into which gas-sand reservoirs can generally be divided based on their AVO characteristics. These classes are referred to in the paper as:

Class 1 high-impedance sands,
Class 2 near-zero impedance contrast sands, and
Class 3 low-impedance sands.

The core of this paper is divided into two parts. The first part describes the range of AVO effects that occur for gas-sand relections; the second part presents the examples. The discussion in the first part uses the Zoeppritz (1919) *P*-wave reflection coefficient for an elastic interface to describe the AVO characteristics of gas sands in three classes. Only interface reflectivity is considered in the analysis. Thin-bed effects, attenuation, and other propagation factors well known to influence AVO measurements are not considered. The discussion and analysis concerning the three classes are useful and valid in a general sense but are not meant to replace detailed seismic modeling, which is an indispensable part of AVO analysis.

The Class 1 example involves a Pennsylvanian age channel sand in the Arkoma Basin. The examples corresponding to the second and third classes involve a Miocene age gas sand from the Brazos offshore area and a Pliocene age gas sand from the High Island offshore area, respectively.

Our reasons for focusing on gas-sand reflections in this work are twofold: (1) The majority of the AVO work being done by interpretation geophysicists today involves gas-sand reflections. (2) The contrast in Poisson's ratio between a gas sand and the encasing medium is usually large, meaning that gas sands have detectable changes in amplitude with offset. These amplitude changes allow us to loosely group gas-sand reflections into the three classes described above. This same

Manuscript received by the Editor October 7, 1988; revised manuscript received December 16, 1988.
*Formerly Tenneco Oil Company; presently Anadarko Petroleum Corporation, 16801 Greenspoint Park Drive, Houston, TX 77060.
‡Tenneco Oil Company, P.O. Box 2511, Houston, TX 77252-2511.

type of grouping for oil-sand reservoirs and carbonate reservoirs is usually not possible since their contrasts in Poisson's ratio with the encasing media are generally smaller and less predictable than those for gas sands. Our intent in this paper is to present a loose classification scheme that explorationists can use to "mentally model" the AVO response of gas-sand reflections as the first step in a more rigorous AVO analysis. Explorationists can use the concepts presented here to predict the characteristics of a gas-sand reflection on stacked data and to make a preliminary determination of the type and detectability of its AVO response.

RANGE OF AVO EFFECTS IN GAS SANDS

The range of AVO effects for sandstone reservoirs is analyzed with the Zoeppritz P-wave reflection coefficient. Our model for the gas-sand reservoir is a simple one consisting of a gas-filled sand encased in shale. Figure 1 is a schematic diagram that shows the upper interface of this reservoir model. Figure 2 shows a set of reflection coefficient AVO curves for this interface calculated for a range of normal incidence reflection coefficient R_0. The reflection coefficient curves corresponding to the reverse situation, i.e., a gas sand-shale interface, are approximately mirror images of the curves in Figure 2. Ostrander (1984) presents a similar analysis of gas sands employing suites of reflection coefficient curves like those in Figure 2; however, his analysis is more focused on Class 3 sands.

The curves in Figure 2 were computed for Poisson's ratios of the shale and gas sand of 0.38 and 0.15, respectively and densities of the shale and gas sand of 2.4 and 2.0 g/cm^3, respectively. Of course, one would not expect the Poisson's ratios and density contrasts for a shale-gas sand interface to remain constant over such a wide range of R_0 values. Nevertheless, if we assume large Poisson's ratio contrasts, the qualitative analysis we present in this paper is not sensitive to precise values for Poisson's ratio and density contrasts.

The AVO curves of Figure 2 can be loosely divided into the three classes as marked in the display: high-impedance sands (Class 1), nearly same as shale impedance sands (Class 2), and low-impedance sands (Class 3). The reflection characteristics of these three classes are discussed in the following subsections. The possible AVO responses for a shale-gas sand interface form a continuum. We make no attempt to establish hard

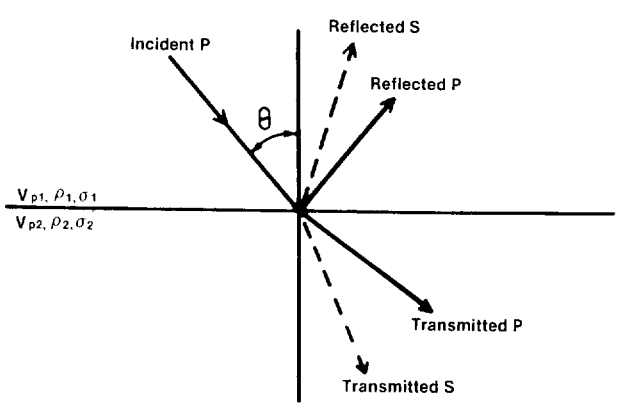

FIG. 1. Schematic diagram of a shale-gas sand interface.

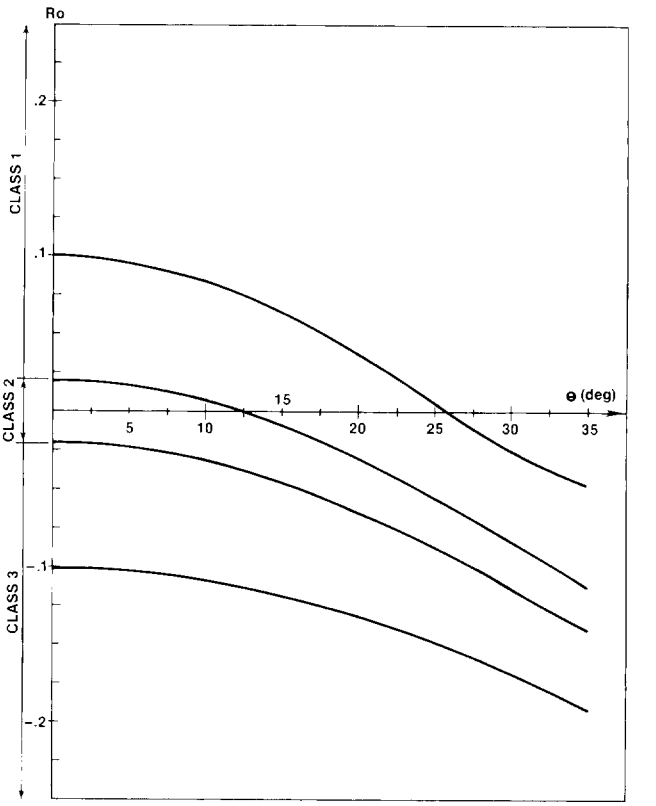

FIG. 2. Zoeppritz P-wave reflection coefficients for a shale-gas sand interface for a range of R_0 values. The Poisson's ratio and density of the shale were assumed to be 0.38 and 2.4 g/cm^3, respectively. The Poisson's ratio and density of the gas sand were assumed to be 0.15 and 2.0 g/cm^3, respectively.

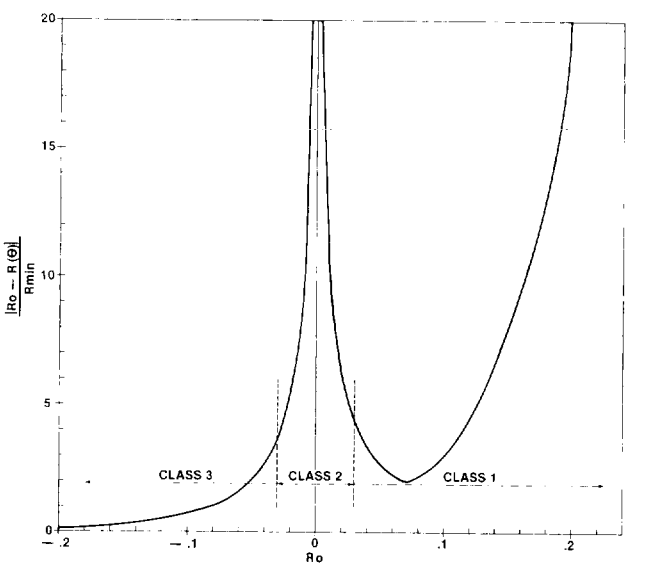

FIG. 3. Fractional change in reflection coefficient for a shale-gas sand interface over an angular range of 0 to 30 degrees. The fractional change is given by $|R_0 - R(30\text{ deg})|/R_{min}$, where R_{min} is the lesser of $|R_0|$ and $|R(30\text{ deg})|$.

lines of demarcation between the gas-sand reflector classes in this paper. Instead, we propose fuzzy boundaries in terms of normal-incidence impedance contrasts that create ranges in the continuum of AVO responses with similar characteristics.

Class 1—High-impedance sands

A Class 1 sand has higher impedance than the encasing medium, usually shale. A shale-sand interface for these sands has a fairly large, positive R_0. The top curve in Figure 2 is representative of a Class 1 sand, which is usually found onshore in hard rock exploration areas. It is a mature sand which has undergone moderate to high compaction.

The reflection coefficient of a high-impedance sand is positive at zero offset and initially decreases in magnitude with offset. The magnitude of the rate of change of amplitude with offset (referred to as the "gradient") for a Class 1 sand is usually greater than that for a Class 2 or Class 3 sand. The gradient depends on R_0, as well as the Poisson's ratio contrast across the interface. In general, the gradient decreases as R_0 decreases for a decrease in Poisson's ratio. [The interested reader can quantify these characteristics by referring to Shuey (1985) and Koefoed (1955)].

The magnitude of the reflectivity of a Class 1 sand initially decreases with offset and can change polarity if adequate angle/offset range is available. Hence, in the best case, normal-incidence synthetic seismograms do not accurately predict the amplitude of the reflection response of Class 1 sands on stacked data. If polarity changes are pronounced, the reflection response of a Class 1 sand can cancel in CMP stacking or can have polarity opposite to that predicted by normal-incidence modeling.

Since the zero-offset reflection coefficient has high amplitude in Class 1 sands, large fractional changes in amplitude are possible if the far-trace reflectivity is near zero. Hence, dramatic AVO effects are possible. Figure 3 shows the fractional change in reflection coefficient from near to far offset as a function of R_0. The curve in Figure 3 was produced using

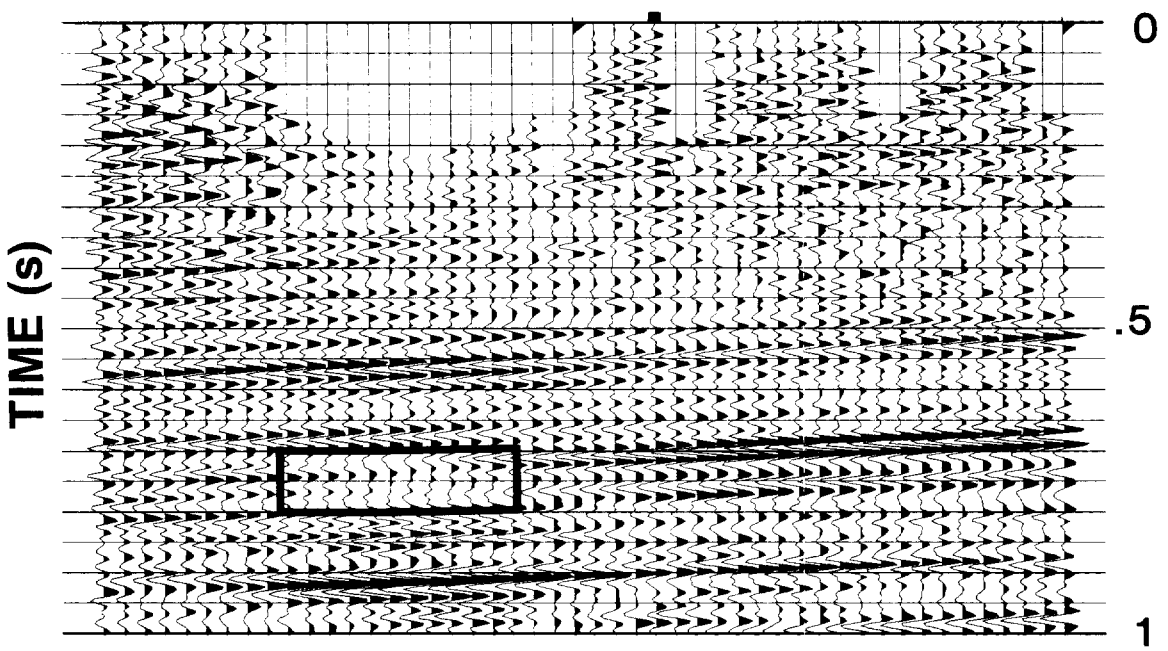

FIG. 4. A stacked section that traverses a productive Hartshorn channel sand. The productive interval corresponds to the dim out which is highlighted in the figure. The dim out is caused by a change in polarity with offset of the Hartshorn reflection, that causes cancellation upon CMP stacking.

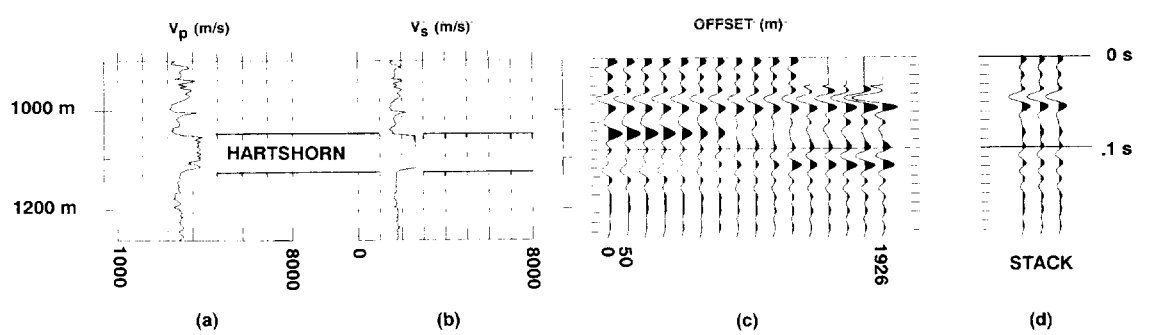

FIG. 5. Modeling a CMP gather. (a) *P*-wave sonic log through the productive Hartshorn interval. (b) Estimated *S*-wave sonic log. (c) The computed CMP gather. (d) Stack of the traces in (c).

the Shuey (1985) approximation to calculate $\Delta R(\theta_m)$,

$$\Delta R(\theta_m) = \frac{|R_0 - R(\theta_m)|}{|R_{\min}|}, \quad (1)$$

where $R(\theta_m)$ is the reflection coefficient at reflection angle θ_m and $|R_{\min}|$ is the lesser of $|R_0|$ and $|R(\theta_m)|$. Hence, the fractional change is referenced to the near- or far-trace reflectivity, whichever is smaller in magnitude. Note in Figure 3 the large fractional changes in reflectivity that are possible for Class 1 sands, particularly those associated with large values of R_0.

Class 2—Near-zero impedance contrast sands

A Class 2 sand has nearly the same impedance as the encasing material. Such a sand is generally moderately compacted and consolidated. The middle two curves in Figure 2 represent a range of possible AVO responses in Class 2 sands.

Since the zero-offset reflection coefficients of Class 2 sands are close to zero, large fractional changes in reflectivity from near to far offset can occur (see Figure 3), enhancing the detectability of these sands. The gradients associated with Class 2 sands are usually large in magnitude but are generally less than those for Class 1 sands. The small offset reflectivity of Class 2 sands is close to zero and is often undetectable in the presence of noise. The reflections seem to suddenly appear at larger offsets when the reflection amplitudes rise above the noise level.

A polarity change occurs if R_0 is positive, but it is usually not detectable, because it occurs at a near offset where the signal is below the noise level.

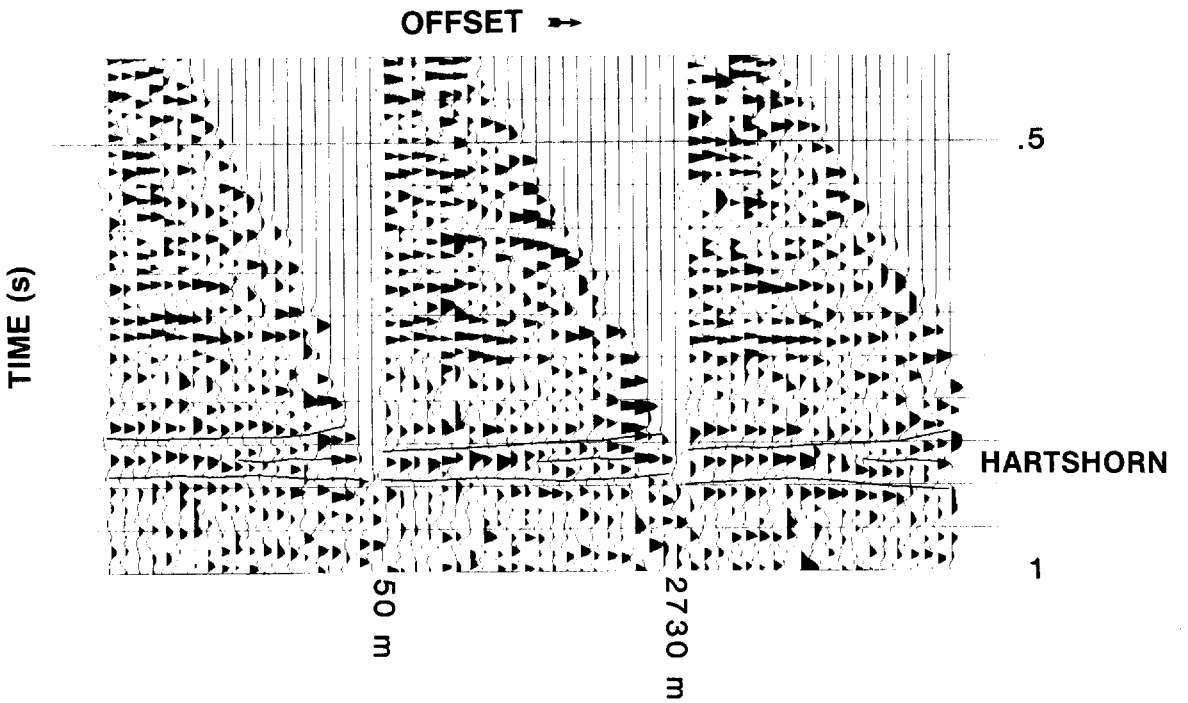

FIG. 6. Three adjacent CMP gathers that show the polarity change associated with the Hartshorn gas-sand reflector. The last few traces in the gathers at far offsets are distorted by NMO stretch.

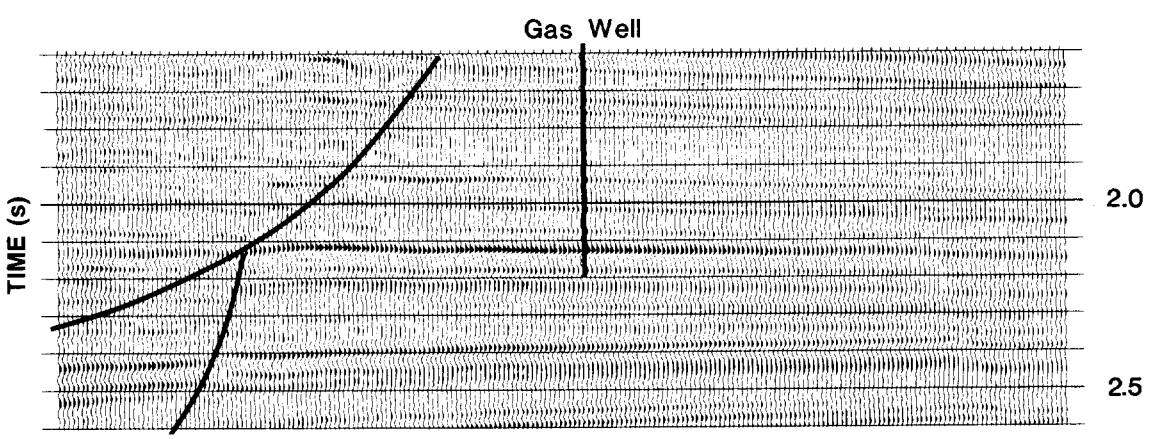

FIG. 7. Migrated, stacked section that traverses a Miocene gas sand in the Brazos offshore area of the Gulf of Mexico. The reflector of interest is at about 2.1 s on the section.

Class 2 sands may or may not correspond to amplitude anomalies on stacked data. If adequate angular range is available, the amplitude buildup with offset is often enough to produce an anomalous response on stacked data. Miocene sands in the Gulf of Mexico frequently exhibit this characteristic. Normal-incidence synthetic seismograms are totally inadequate to describe the response of Class 2 sands on stacked seismic data. Seismic inversion techniques employing stacked data are also highly questionable for these sands.

Class 3—Low-impedance sands

A Class 3 sand has a lower impedance than the encasing medium. Such a sand is usually undercompacted and unconsolidated. Plio-pliestocene sands in the Gulf of Mexico are typically Class 3 sands. Many of the early uses of AVO involved validating amplitude anomalies associated with Class 3 gas sands.

Class 3 sands have amplitude anomalies on stacked seismic data and have large reflectivities at all offsets. Their gradients are usually significant but of lower magnitude than those of Class 1 and 2 sands, since their normal-incidence reflection coefficients are already negative. Class 3 sands do not generally have large fractional changes in amplitude from near to far offset (see Figure 3). In some situations, the amplitude change with offset is small enough that it is not detectable because of tuning, attenuation, recording array, and signal-to-noise ratio decreases with offset. Hence, Class 3 sands sometimes have a high-amplitude response that is relatively flat with offset.

Polarity changes are not associated with Class 3 sands. Hence, CMP stacking does not produce catastrophic effects, and normal-incidence synthetic seismograms generally provide adequate character matches with stacked data. CMP stacking still misrepresents the zero-offset response and can be inappropriate for use in seismic inversion; however, the effects are not as pronounced as for Classes 1 and 2.

EXAMPLES

This section presents examples of the AVO characteristics of Class 1, 2, and 3 gas sands. The specifics of the data processing sequences used to generate the examples are beyond the scope of this paper. Obviously, proper seismic data processing is critical to the successful implementation of AVO analysis. The goal of seismic data processing for AVO is to preserve amplitude variations with offset while removing the effects of spherical spreading, attenuation, transmission loss, signal-to-noise ratio (S/N) decrease with offset, and other propagation factors—a difficult job at best. The seismic displays used in the examples were produced using processing techniques that follow guidelines suggested by Yu (1985).

Class 1 sand AVO example

The first example is taken from the Arkoma Basin and involves the Pennsylvanian age Hartshorn sand. Thick Hartshorn channel sands that are shallow (about 1000 m) can be prolific producers. In the past, geophysicists exploring the Hartshorn have noticed that "dim outs" in the Hartshorn reflection occur when a thick, gas-filled Hartshorn channel

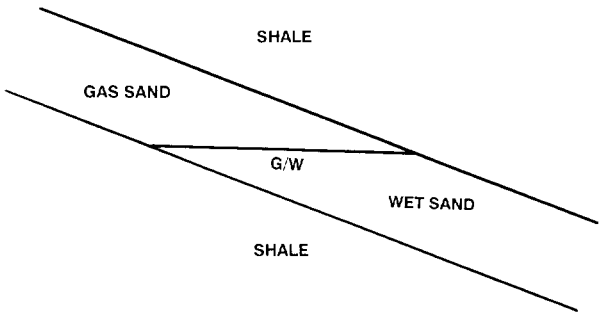

FIG. 8. Schematic diagram of the Brazos gas sand.

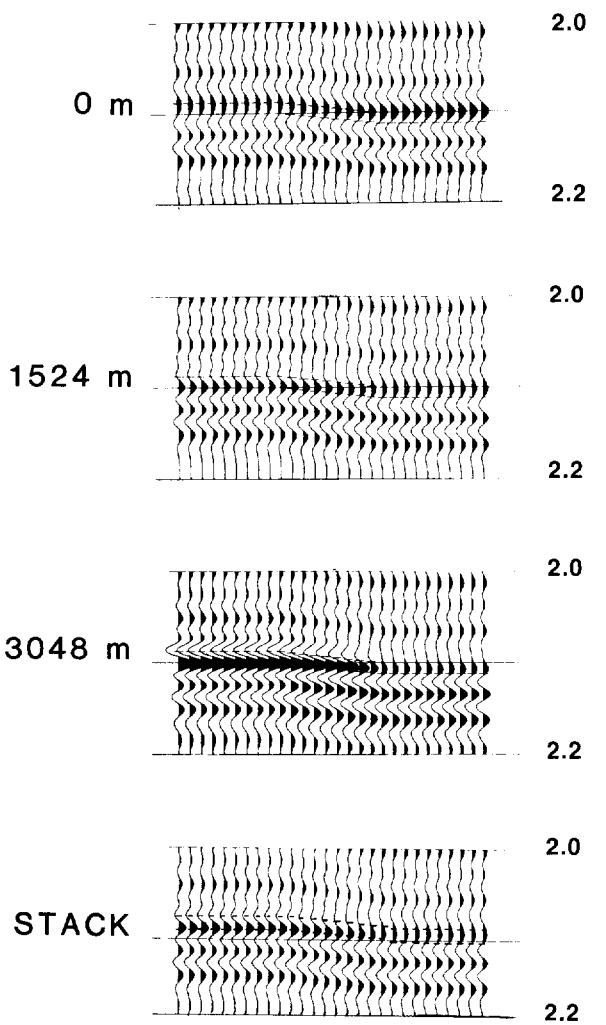

FIG. 9. Synthetic cross-sections corresponding to the model of Figure 8 were computed using logs from a well that tested the Miocene gas sand shown in Figure 7. The top three cross-sections correspond to offsets of 0 m, 1524 m, and 3048 m. The lower cross-section was produced by stacking the range of offsets used to form the data in Figure 7.

configuration develops. Figure 4 shows an example of this dim out effect in a productive Hartshorn channel sand.

Normal-incidence modeling does not describe the dim out phenomenon. Figure 5c shows a synthetic CMP gather calculated using well logs that penetrated a thick, gas-filled Hartshorn channel sand. (Unfortunately, the logs shown in Figures 5a and 5b do not correspond to the seismic data shown in Figure 4. The logs corresponding to the data of Figure 4 were unavailable.) The first trace on the left in Figure 5c is the normal-incidence trace. The second trace corresponds to an offset of 50 m, and the remaining traces increment in offset by 134 m. The offset geometry used in Figure 5c is typical of the seismic data used for Hartshorn exploration in the Arkoma Basin. The stack of the traces in Figure 5c is shown in Figure 5d.

The sonic log in Figure 5a reveals that the Hartshorn sand package is definitely a Class 1, high-impedance sand. The normal-incidence synthetic seismic trace also predicts that the top and base of the Hartshorn correspond to strong reflections, which is opposite to what is observed on stacked seismic data. The AVO response for the Hartshorn predicted by the model in Figure 5c explains the paradox. A polarity change occurs at about the middle offset and produces nearly perfect cancellation by CMP stacking.

Figure 6 displays three adjacent CMP gathers corresponding to the dim out area of Figure 4. Note the polarity change that occurs in the mid-range of offsets. To enhance the visual detectability of the Hartshorn polarity change, the traces in Figure 6 are displayed in reverse polarity with respect to the model traces of Figure 5c. Even though the model in Figure 5c corresponds to a different Hartshorn reservoir, the model qualitatively explains the AVO behavior of Figure 6.

The information presented in Figures 4 through 6 explains the dim out phenomenon observed in gas-filled Hartshorn channel sands in the Arkoma Basin. The figures also reveal that the dim out effect is a fortuitous combination of reflector depth and seismic data acquisition geometry. For deeper or shallower Hartshorn sands, the polarity change would shift away from the mid-offsets and could produce a quite different stacked response, suggesting the need to model accurately the acquisition geometry and reflector depth when exploring for Class 1 sands that are likely to have polarity changes. Instead of conventional stacked sections, limited offset or constant-angle seismic sections should be used to enhance detectability.

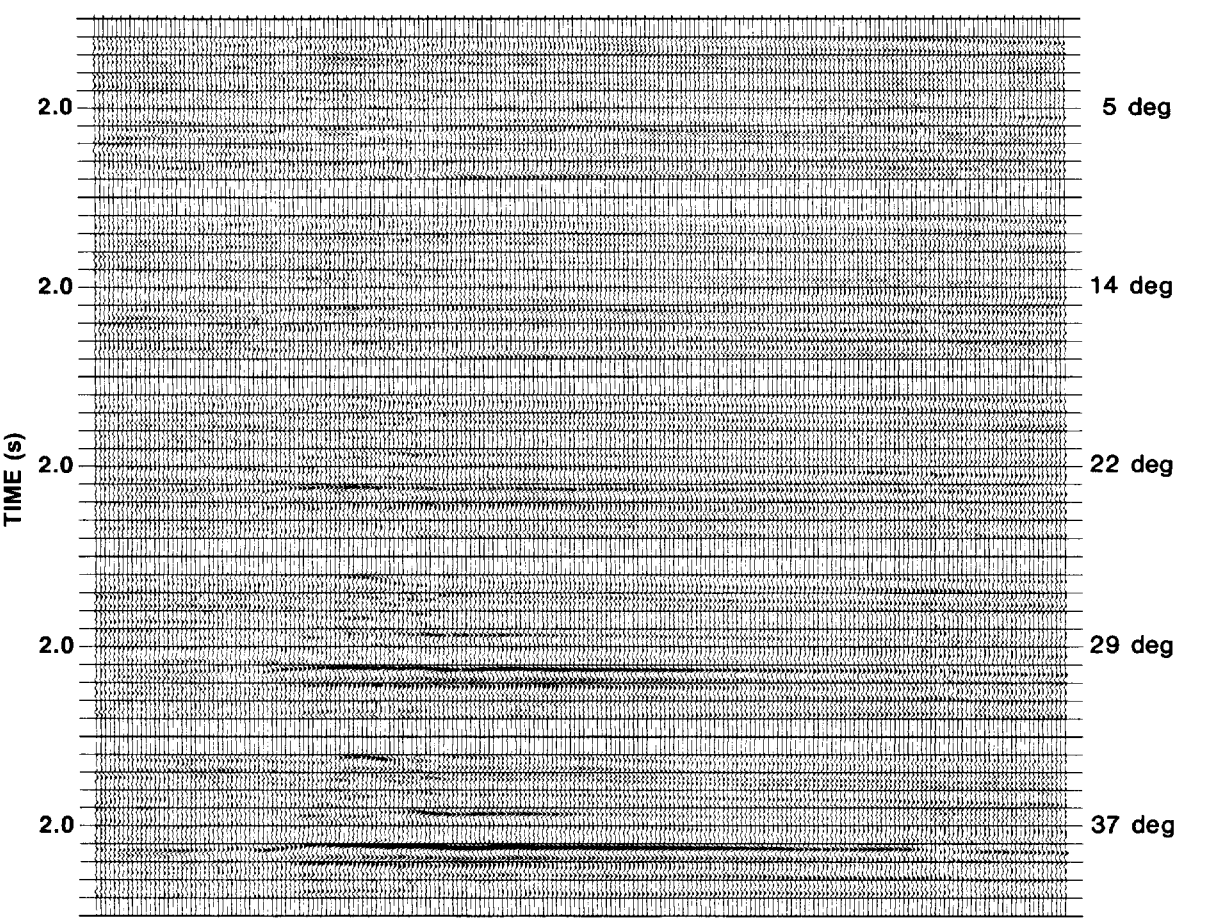

FIG. 10. Panel display of constant reflection angle sections corresponding to Figure 7. The angles posted on the right side of the figure refer to the centers of the reflection angle ranges in each panel. Each 1.0 s panel displays 1.6 s to 2.4 s of live data.

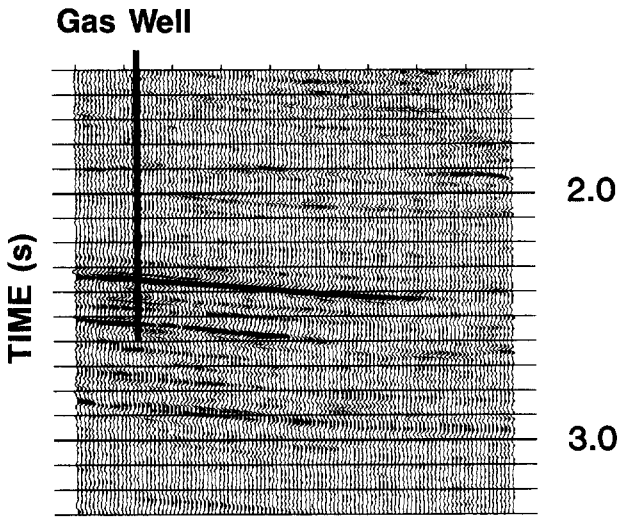

FIG. 11. Migrated, stacked section that traverses a Pliocene gas sand in the High Island area of the Gulf of Mexico. The reflector of interest is between 2.3 s and 2.5 s.

Class 2 sand AVO example

The second AVO example concerns a mid-Miocene age sand from the Brazos area of the Gulf of Mexico. Figure 7 is a stacked section showing the reflection from this gas sand. The gas-sand reflection (at about 2.1 s) is anomalous in character but is not the classic type of amplitude anomaly one usually associates with the Gulf of Mexico. The reflection from this gas sand defies explanation with conventional, normal-incidence modeling.

Figure 8 is a schematic model believed to correspond to the gas-sand reservoir in Figure 7, and Figure 9 shows a corresponding set of synthetic seismic cross-sections, computed from the Zoeppritz equations. AVO effects are accurately modeled. The first ten traces on the left of each display are identical and were calculated from well logs that penetrated the productive mid-Miocene gas-sand reflector shown in Figure 7. The last ten traces on the right of each display are identical and were calculated from the same well logs altered to model water-saturated sand. The intervening traces were calculated from well logs interpolated to model the flat (in depth) gas-water contact shown in Figure 8.

Note the lack of correlation between the normal-incidence synthetic seismic cross-section and the anomalous reflection response of the gas-filled sand. The normal-incidence model predicts an amplitude dimming to be associated with the presence of gas. In the past, most geophysicists—including the authors—would have been tempted to assume that the sonic and density logs were in error and lower the impedance of the sand to explain the higher amplitude associated with gas.

The mid-offset (1524 m) and the far-offset (3048 m) synthetic cross-sections reveal that AVO effects associated with the gas sand are quite pronounced. The anomalous character of the gas sand on the stacked data in Figure 7 is caused by large far-trace amplitudes. The stacked cross-section in Figure 9 predicts an anomalous response for the gas sand similar to that seen in Figure 7.

Figure 10 is a panel display of constant reflection angle sections. Each panel in Figure 10 corresponds to data from Figure 7 stacked to preserve a different narrow range of reflection angles. Note the excellent qualitative agreement between the predictions of Figure 9 and the constant-angle panels shown in Figure 10. The small-angle reflectivity of the gas sand is close to zero, as is characteristic of Class 2 sands. The gradient is pronounced and gives rise to large reflection amplitudes at the larger reflection angles. The detectability of this sand is enhanced through the use of displays similar to Figure 10 as opposed to stacked data displays like Figure 7.

Class 3 sand AVO example

The final example involves a Class 3 gas sand from the High Island offshore area of the Gulf of Mexico. Figure 11 shows a seismic line that traverses the gas sand. The gas sand is Pliocene in age and has a pay thickness in excess of 30 m. The gas sand is associated with the classic bright spot seen on Figure 11.

The Class 3 gas-sand AVO characteristics are easily seen in the constant reflection angle panels of Figure 12. The small-angle reflection strength is fairly large. The fractional change in reflection strength from small to large reflection angles is detectable but not large compared to those of the Class 1 and 2 examples previously discussed. All reflection angles contribute significantly to the stacked response seen in Figure 11.

Class 3 gas sands like the Pliocene sand in Figures 11 and 12 are often subjects of AVO analysis primarily for two reasons: (1) these sands are the easiest to find on the stacked data that most interpreters use and (2) S/N as a function of offset for these sands is usually adequate for AVO analysis.

Class 3 sands have fairly large reflectivities at all offsets and no polarity changes; hence, their detectability on stacked data is not sensitive to acquisition geometry. This is not to say that all acquisition geometries are adequate for AVO analysis, since subtle changes in amplitude with offset require large ranges of offsets to detect. Class 1 and 2 sands, on the other hand, can be difficult to detect on stacked data because of combinations of AVO effects and acquisition geometries.

Adequate S/N as a function of offset and a sufficiently large offset range are extremely important in AVO analysis. S/N of seismic data typically decreases monotonically with offset. AVO analysis applied to data without adequate S/N over a sufficient offset range usually fails. Since Class 3 sands are bright at near offsets and brighten with offset, they offer the best chance of having adequate S/N as a function of offset for AVO analysis.

SUMMARY

This paper proposes a classification of gas-sand reflections based on their AVO characteristics and presents seismic data examples illustrating these characteristics. Three classes of gas-sand reflections are proposed in the paper.

A Class 1 sand is generally found in a hard-rock, onshore area and has a higher impedance than the encasing shale material. Class 1 sands, such as the Hartshorn channel sand example, can have polarity changes associated with them that produce dim out effects in stacked seismic data.

Class 2 sands are found in onshore and offshore exploration

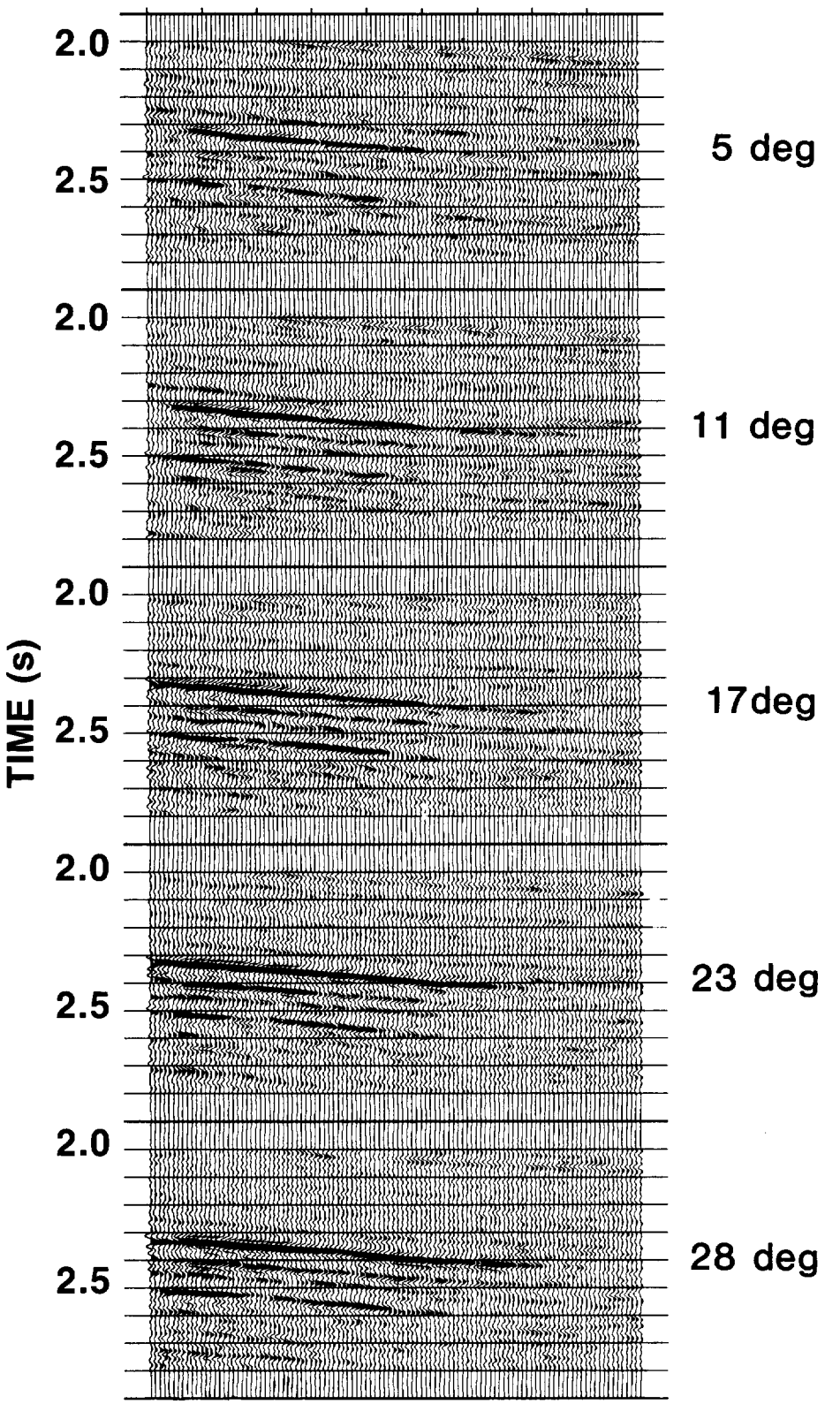

FIG. 12. Panel display of constant reflection angle sections corresponding to the data of Figure 11. The angles posted on the right side of the figure refer to the centers of the reflection angle ranges in each panel. Each 1.0 s panel displays 2.0 s to 2.8 s of live data.

areas. They have almost the same impedance as the encasing shale. Class 2 sands can have dramatic AVO effects if adequate angle/offset range is available in the seismic data. The stacked response of Class 2 sands, such as the Miocene age gas-sand example from the Brazos offshore area of the Gulf of Mexico, comes mainly from the far offsets.

Class 3 sands are found mainly in marine environments. They have lower impedances than the encasing shale. Pliopleistocene gas sands, such as the High Island example from the Gulf of Mexico, are usually Class 3 sands. The AVO characteristics of Class 3 sands are usually less pronounced than those of Class 1 and 2 sands but are often more amenable to AVO analysis because of S/N considerations.

ACKNOWLEDGMENTS

The authors of this paper gratefully acknowledge Tenneco Oil Company for permission to publish this paper. We also acknowledge Tom Heinecke, Joanna Sixta, and Dave Godwin for their seismic interpretation work on the three examples presented in the paper. Special thanks are given to Pat Townsend, Robert Benavidez, and Cheryl Troesser for processing the AVO examples and their assistance in preparing seismic displays for the figures. We also wish to express our thanks to Don Frye and David Jenkinson for reviewing the manuscript and suggesting revisions. Synthetic sections shown in this paper are produced by the Daniel Geophysical[1] software package.

REFERENCES

Koefoed, O., 1955, On the effect of Poisson's ratio of rock strata on the reflection coefficients of plane waves: Geophys. Prosp., **3**, 381–387.

Ostrander, W. J., 1982, Plane-wave reflection coefficients for gas sands at non-normal angles of incidence: 52nd Ann. Internat. Mtg., Soc. Expl. Geophy., Expanded Abstracts, 216–218.

——— 1984, Plane-wave reflection coefficients for gas sands at non-normal angles of incidence: Geophysics, **49**, 1637–1648.

Shuey, R. T., 1985, A simplification of the Zoeppritz equations: Geophysics, **50**, 609–614.

Yu, G., 1985, Offset-amplitude variation and controlled-amplitude processing: Geophysics, **50**, 2697–2708.

Zoeppritz, K., 1919, Erdbebenwellen VIII B, Uber Reflexion and Durchgang seismischer Wellen durch Unstetigkeitsflachen: Gottinger Nachr., **1**, 66–84.

[1]Daniel Geophysical Company is a wholly owned subsidiary of Daniel Industries of Houston, Tx.